6. Thermal-Hydrological-Chemical Processes

Chapter 6 includes a discussion of Integrated Assessment of Chemical Measurements and Numerical Analyses.

6.1 Integrated Assessment of Chemical Measurements and Numerical Analyses

6.1.1 Overview

Discussions on geochemistry for the thermal testing program focused on integration of geochemical data and thermal-hydrological-chemical (THC) modeling into Performance Assessment. The four major areas of discussion were: (1) Integration and application of THC models for PA, (2) Gas-phase CO_2 and isotope chemistry, (3) THC model integration and update of THC models with comparison to gas and liquid chemistry, and (4) Sidewall coring mineralogy. Other areas of discussion included the heating schedule for the DST, planning for further geochemical sampling at the DST, and planning regarding the design of the Cross Drift Thermal Test.

6.1.2 Integration of THC Modeling into Performance Assessment

Recently, several major inputs to Performance Assessment and other YMP project documents have been provided based on models of THC processes. Although most geochemical data from the DST are not used directly in the THC models (except for the initial pore water chemistry) the DST remains the most important validation test for the THC models.

The goals of the models used for prediction of drift-scale THC processes and their abstraction are:

- Provide a conceptual basis and methodology for developing drift-scale THC models

- Validate the THC model by comparing its results to results from field (i.e. thermal testing) and laboratory experiments

- Identify conceptual uncertainties and address uncertainty through sensitivity studies that vary key parameters

- Predict changes in hydrologic properties resulting from mineral precipitation/dissolution and associated THC effects on flow and seepage

- Predict changes in water and gas chemistry around drifts, which are the potential elements that could enter drifts through seepage or gas flow.

A list of major project documents where THC modeling and model validation to the DST are discussed is as follows:

- AMR N0120 "Drift-Scale Coupled Processes (DST and THC Seepage) Models" Rev. 01 ICN 01 (BSC 2001)
- UZ PMR
- NFE PMR
- SSPA Volume 1
- NRC KTI - DOE Agreements
- PSSER
- FEPs
- Abstractions for TSPA-SR (seepage water and gas chemistry, effects on flow)

Detailed discussion of the results of the THC models for PA are discussed primarily in the SSPA Volume 1 (Sections 3.3.6, 4.3.6, and 6.3.1) and in AMR N0120 Rev. 01 and are not repeated here. Figure 153 illustrates the general relationship between the DST THC models and geochemical data and the THC models used for PA.

6.1.3. Isotopic Analyses of Gas and Water Samples from the Drift Scale Test

Field Sampling

Two additional sets of gas and vapor condensate samples were collected from the hydrology boreholes since the last thermal test workshop (October, 2000). Analyses of the amount and stable carbon isotopic compositions ($\delta^{13}C$) of CO_2 in the gas samples and the hydrogen (δD) and oxygen ($\delta^{18}O$) isotope compositions of the condensate samples are complete. In addition, most of the analyses of water vapor condensate samples collected during prior sampling periods have also been finished.

CO_2 Data

In general, we have observed that the concentration of CO_2 in the gas samples collected from the DST increase with temperature until the boiling point (~97°C) is reached. Above the boiling point, the concentrations drop off significantly. This is consistent with evolution of CO_2 from the dissolved inorganic carbon (DIC) in the pore water in the rocks during heating up to the boiling point. This is supported by a general trend towards higher $\delta^{13}C$ values as the CO_2 concentrations increase, indicating progressive loss of CO_2 gas (which has lower $\delta^{13}C$ values) from the DIC (which has higher $\delta^{13}C$ values). Once the rock passes through boiling, the pore water is gone and all the DIC has been converted to CO_2 or precipitated in secondary carbonate minerals.

Currently, most of the gas sampling intervals in the DST are above boiling point of water and the CO_2 concentrations are low (<0.2%). However, many of the packers isolating the higher temperature intervals have failed and the gas samples collected from those intervals are a composite of large sections of the monitoring wells. Several of these intervals include sections that are below boiling. As a result, the CO_2 concentrations are considerably higher than expected. For example, the packers separating borehole 78, interval 3 from intervals 1,2 and 4 are all deflated and the measured CO_2 concentration in 78-3 was 0.8% in April, 2001 despite a temperature of 112°C.

In most of the sampling intervals that are still below boiling, the CO_2 concentrations are continuing to increase (the highest measured concentration in April, 2001 was 7.9% in interval 185-2). The most notable exceptions to this are intervals 74-3 and 75-3 (the two highest intervals above the central part of the heater drift). The CO_2 concentrations have dropped off considerably over the last year. Presumably, this indicates a general depletion of DIC in the pore water in the central area of the heated rock.

Water Vapor Condensate Data

In sampling intervals above 50°C, samples of water vapor condensed from the gas have been collected for hydrogen and oxygen isotopic analyses. Using published relationships between vapor and liquid, we can calculate the isotopic composition of the pore water in the vicinity of the sampling interval from the isotopic composition of the vapor.

Since water vapor has lower δD and $\delta^{18}O$ values than co-existing liquid water, these data provide a measure of the degree of water vaporization and condensation occurring in the area of the sampled interval. In general, we have observed that the isotopic composition of the pore water remains approximately equal to the initial $\delta^{18}O$ value of the pore water (–11‰) up to ~90°C. Once the temperature approaches the boiling point, the degree of vaporization of the pore water becomes significant and the isotopic values increase. Exceptions to this include areas where condensed water vapor has been added to the pore water, either by draining through fractures (e.g., beneath the drift in intervals such as 78-3) or where water vapor generated in the boiling zone condenses in the rock above the boiling front and mixes with the pore water (e.g., interval 75-3). In these cases, the low-$\delta^{18}O$ condensate causes the overall isotopic composition of the pore water to decrease. These effects are demonstrated by the data plotted in Figure 154. The oxygen isotopic composition of the pore water around interval 59-3 is equal to or slightly lower than the –11‰ until the temperature in the interval exceeds 93°C. Then the $\delta^{18}O$ value of increases to approximately –6‰ as the rock dries out. In interval 58-3 (~4 m above 59-3), the $\delta^{18}O$ value of the pore water is about –11‰ until the condensate from the boiling front begins accumulating in the rock and the $\delta^{18}O$ value of the pore water drops to approximately –14‰.

6.1.4. DST THC Model Updates and Comparison to New Data

Since the last thermal test workshop, the DST THC model has undergone minor updates, and comparisons to several measurements of water and gas chemistry wee presented in the previous thermal test workshop progress report. No new water chemical data were available at the time of the workshop and therefore no further comparisons are made here. Hence, the discussion on DST THC model results focuses primarily on comparison to the recently collected gas phase CO_2 data.

As discussed in Section 3.2, many of the gas-phase CO_2 analyses are from intervals above the boiling temperature where the packers have been deflated. Thus, these CO_2 data are no longer directly comparable to model results because they represent mixtures of gas from a long interval that crosscuts zones of widely differing temperatures and liquid saturations. Therefore, modeled and measured CO_2 concentrations are shown for only for two borehole intervals (borehole 74, interval 3, and borehole 75, interval 3) where the packers are still intact. For reference, the locations of these borehole intervals and the model grid nodes are shown in Figure 155.

Figure 156 depicts models results from model grid nodes on both the hotter and cooler sides of borehole 74 interval 3, as there are no grid nodes near the center of the interval. The last measured data points (January and April 2001) were determined using a standard concentration that yields values about 15% higher than the previous samples, and although they appear to show nearly constant CO_2, are actually relatively lower in concentration than those collected previously. A consistent recalibration of all the CO_2 concentrations will be done to make the analyses directly comparable. Considering that the earlier analyses should be somewhat higher, the trend in measured compositions is quite similar to the average trend of the model concentrations, that can be inferred from the individual trends. The main difficulty in capturing the later time trend is that the concentrations in the hotter interval are dropping rapidly, whereas those in the cooler interval have only begun to level out.

Measured and modeled CO_2 concentrations from borehole 75 interval 3 are shown in Figure 157. Here the modeled concentrations closely capture the magnitude and trend in concentrations observed up to April 2001. Both results show the strong depletion in CO_2 as the boiling front is advancing toward the interval and as the matrix pore waters are stripped of CO_2 through vaporization and transport to cooler areas.

6.1.5 Mineralogic Analysis of Drift Scale Test Sidewall Cores

In November, 2000, a new sidewall coring tool was used to collect six sidewall cores from inclined boreholes 53 (ESF-HD-CHE-2) and 54 (ESF-HD-CHE-3) while the thermal test was in progress. This capability is a significant improvement over the sampling options for the Single Heater Test, in which overcore samples were collected for mineralogic analysis only after the block had cooled down.

Target Selection

The target locations for sampling were selected on the basis of thermal data and predictions and examination of borehole televiewer logs. Borehole intervals with visible fracturing were chosen to maximize the likelihood of finding mineral deposits resulting from water-rock interaction during the test. The locations targeted for sampling in borehole 54 are within the boiling zone as it existed in November, 2000. It is important to note that these locations existed within the condensation zone above the boiling zone until the boiling zone moved outward to intersect borehole 54, so that observed test effects may be composites of condensation-zone and boiling-zone processes. Borehole 53, higher in the test block than borehole 54, is in the condensation zone and has not experienced temperatures at or above boiling.

Sample Recovery

Six core samples were collected during the inaugural deployment of the sidewall coring tool. The recovered cores received a preliminary examination by stereomicroscopy. Two of the samples from borehole 53 were test targets chosen to evaluate tool performance and were essentially outside the zone of thermal test influence. One such sample contained a natural fracture with no obvious evidence of new mineral deposition. The other sample included a portion of the pre-test wellbore surface, also without evidence of new mineral deposition. These two samples were assigned the lowest priorities for further characterization. A third sample from the condensation zone intersected by borehole 53 also contained only a portion of pre-test wellbore surface without evidence of mineral deposition. This sample was assigned low priority for further characterization, and none has yet been done.

The three samples from borehole 54, collected in two locations where the borehole intersects the boiling zone, all contain evidence of mineral deposition related to the test. The most easily visible deposit is glassy silica scale. One sample also contained minute white, fibrous rosettes of an additional mineral; this sample was selected for detailed examination by scanning-electron microscopy (SEM). For comparison, a sample of pre-test drill core containing a fracture from about the same depth was studied by SEM to provide a baseline inventory of pre-test fracture mineralogy and mineral textures. Chemical compositions of minerals were determined semi-quantitatively by energy-dispersive x-ray spectroscopy.

Basis for Interpretation of Mineral Deposits

The identification of particular mineral deposits as products of water-rock interaction during fluid reflux in the condensation zone, evaporation in the boiling zone, or composites of reflux and evaporation is a matter of interpretation. Salts like calcium carbonate and calcium sulfate are interpreted as products of substantial evaporation. We know that these compounds were deposited in the condensation zone of the Single Heater Test at temperatures below boiling, probably when the rock began to dry out after test completion. This combination of conditions did not exist at sampling time in either the boiling or condensation zones of the Drift Scale Test, and therefore we expect salts to be deposited in the boiling zone and to be products of high-temperature evaporation during dryout.

It is not clear what deposits from the condensation zone might look like. It seemed likely that conductive fractures would receive numerous packets of reflux water and that mineral deposits, probably silica, would have textural features reflecting multiple episodes of deposition. For example, a deposit built up from many layers of silica or built by aggregation of many smaller deposits could be a product of deposition in the condensation zone.

Silica deposits produced only by evaporation in the boiling zone are expected to be thin, with little or no indication of successive buildup. Deposits were expected to be thin because any particular portion of fracture surface would receive deposition only from evaporating water exiting the adjacent rock matrix.

Pre-Existing Natural Fracture Minerals

Pre-test core samples from the depths where sidewall samples were collected were analyzed for natural fracture mineralogy. The natural mineralogy is the baseline for documenting evidence of mineralogic change in fractures during the test. Potential changes during the test might include deposition of new mineral phases and dissolution of pre-existing minerals. In several cases, the pre-test core samples were collected from slightly different depths than the sidewall samples because core at the precisely corresponding depth contained no fractures and therefore was unsuitable for analysis. Some information about pre-existing natural fracture minerals was also obtained from examination of sidewall samples.

The dominant fracture-coating mineral from pre-test core ESF-HD-CHE-3 (hole 54) at the 66.7-ft depth is the calcium zeolite stellerite. Additional minerals include potassium feldspar, crystalline silica, smectite, mordenite, and minor pyrite. The rock matrix exposed on some parts of the fractures is mostly a fine-grained mixture of feldspar and silica minerals.

Test-Related Mineral Deposition

The three products observed so far are tentatively identified as amorphous silica, a calcium sulfate phase (gypsum or anhydrite), and a calcium-rich phase that is probably calcite. The silica deposits exhibit considerable textural heterogeneity, perhaps because some were deposited when the collection site was in the condensation zone and others deposited when boiling-zone dryout conditions were reached.

The images in Figure 158 (file 3) and Figure 159 (file 9) show two examples of possible condensation-zone silica deposits. Figure 158 shows a fracture surface completely coated by terrace-like silica deposits up to a few micrometers thick. In Figure 159, several discoid silica deposits (up to about 20 micrometers across) rest on a surface of earlier-deposited discs cemented and largely obscured by silica particles about one or two micrometers across. In both examples, the deposits were built up during multiple episodes of silica deposition.

Very thin (less than 0.5 micrometer thick), curled silica sheets may be products of final dryout in the boiling zone, Figure 160 (file 17). There is no textural evidence of successive buildup in the silica sheets. Also lying atop the earlier silica deposits or on pre-test fracture surfaces are scattered deposits of prismatic calcium sulfate Figure 161 (file 16) and rounded mounds of probable calcite Figure 162 (file 11).

Evidence of Dissolution

Possible dissolution of natural fracture-coating minerals was observed adjacent to one of the thicker lobate silica deposits interpreted as condensation-zone deposits, Figure 163 (file 4), Figure 164 (file 10). A highly corroded stellerite crystal Figure 164, (pt 2) presents a strong textural contrast to the well preserved prismatic crystal forms away from the silica deposit. Next to the corroded stellerite, a silica crystal, probably cristobalite, also appears corroded Figure 164 (pt 1). The localization of dissolution evidence close to test-related silica deposits suggests that much of the dissolved material is redeposited after very little transport.

6.1.6 Planning for Further Sampling at the DST

Suggestions were made regarding the potential for collecting water in the future. Based on the lack of significant water collected from boreholes and the slow rate of advance of the boiling front it does not appear likely that samples will be collected from the upper hydrology boreholes (e.g., boreholes 58 and 75). Therefore, another potential way of collecting pore water was proposed. This involves drilling through regions of high liquid saturation where matrix inbibition of draining fracture waters has taken place. Direct measurement of liquid saturation will enable estimates of fracture-matrix interaction. Additionally, ultracentrifugation of the pore waters will allow for assessment of matrix pore water dilution as well as give constraints on water-rock interaction.

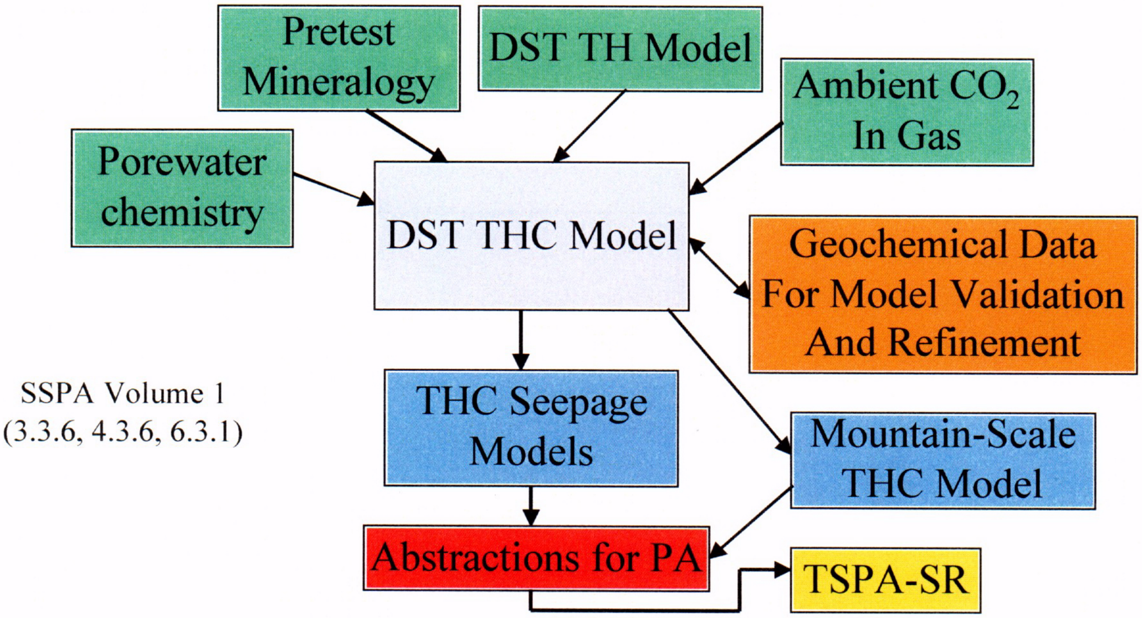

Figure 153. DST THC data, model, and integration into PA.

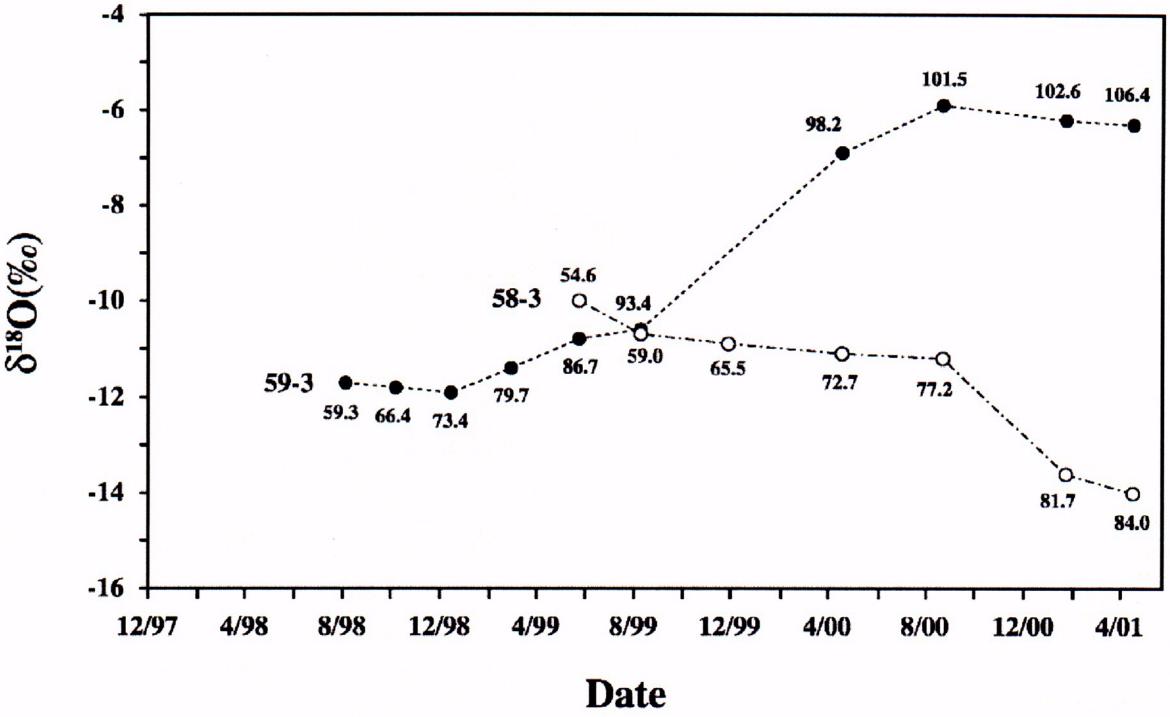

Figure 154. $\delta^{18}O$ values of vapor condensate (re-calculated to represent the oxygen isotope ratio of water in equilibrium with the vapor) collected from interval 3 in boreholes 58 and 59. Also shown are the temperatures (°C) for the intervals at the times the samples were collected.

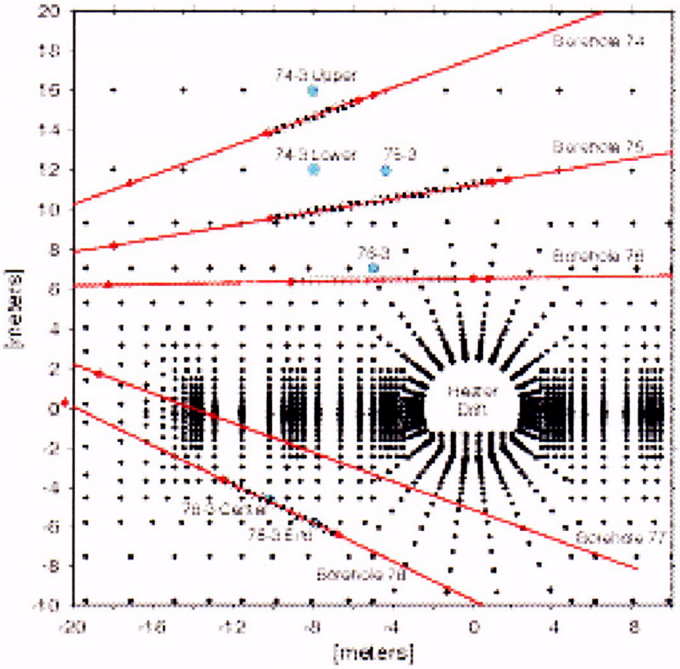

Figure 155. Layout of borehole intervals and DST THC model grid nodes. Colored nodes refer to those used for comparison to CO_2 concentrations.

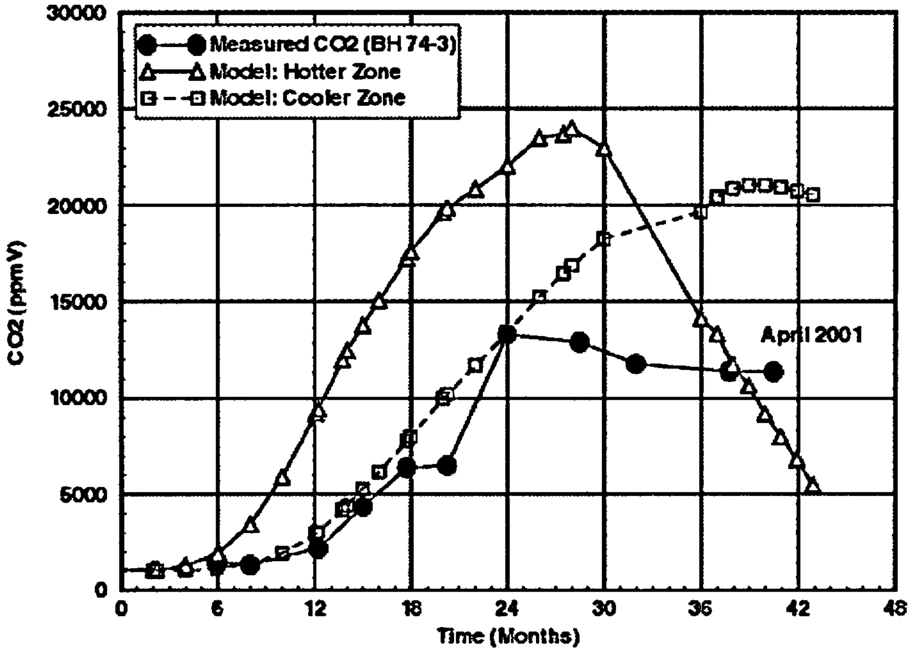

Figure 156. Evolution of measured CO_2 over time from Borehole 74, interval 3 compared to DST THC model results. As a result of coarser discretization in the area of this interval, model results from elements on the hotter and cooler sides are shown.

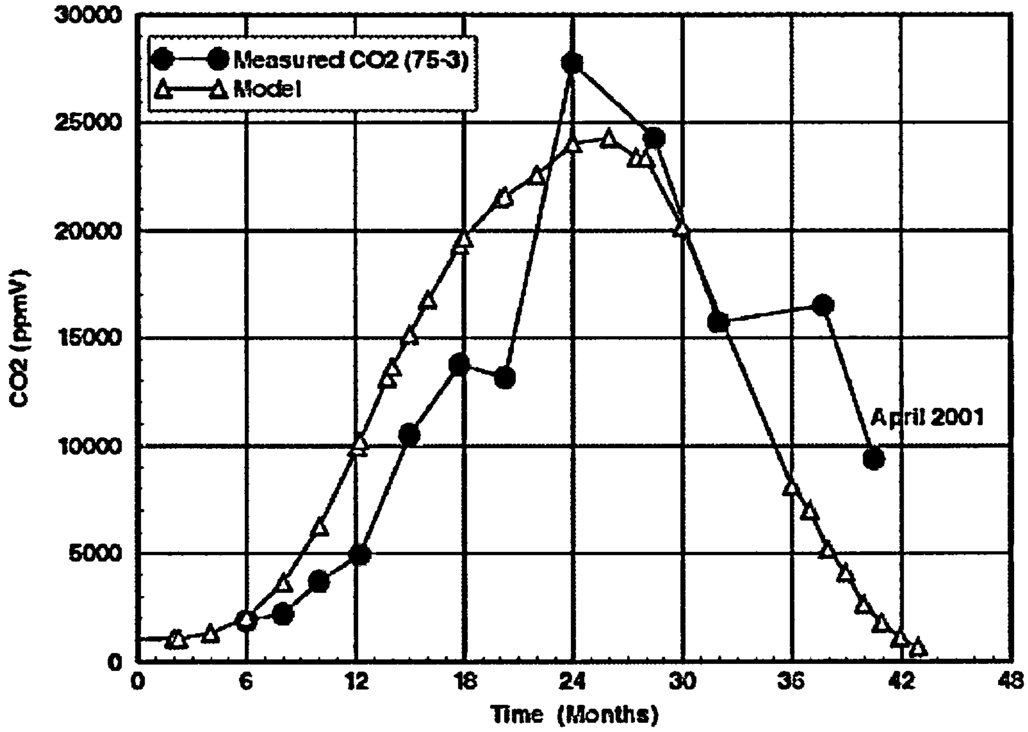

Figure 157. Evolution of measured CO_2 over time from Borehole 75, interval 3 compared to DST THC model results.

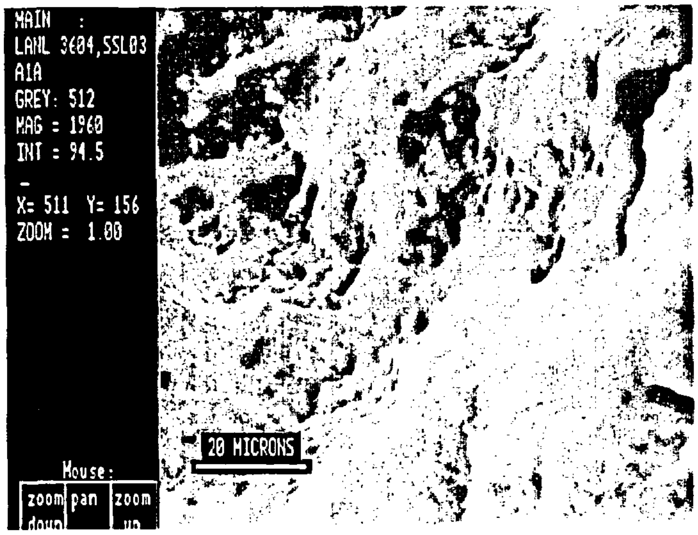
MAIN :
LANL 3604,SSL03
A1A
GREY: 512
MAG = 1960
INT = 94.5
X= 511 Y= 156
ZOOM = 1.00

Figure 158 (file 3) Terrace-like deposits of amorphous silica coating a fracture surface. Secondary-electron image.

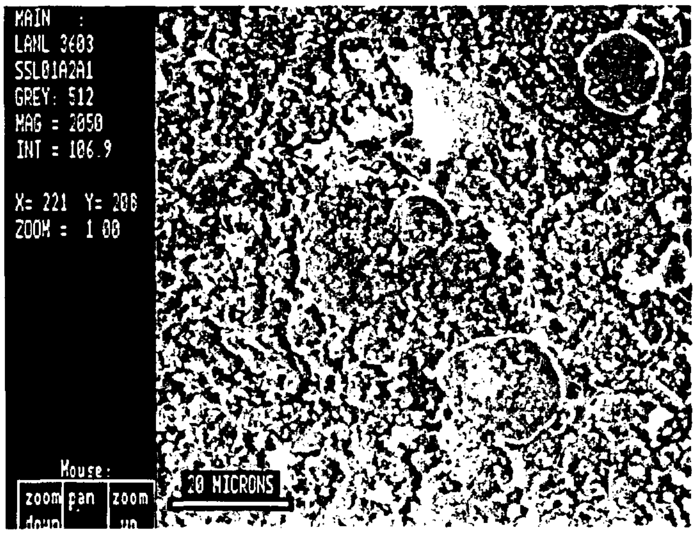
MAIN :
LANL 3603
SSL01A2A1
GREY: 512
MAG = 2050
INT = 106.9
X= 221 Y= 208
ZOOM = 1.00

Figure 159 (file 9). Discoid silica deposits rest on a surface of earlier discs cemented by silica particles. Secondary-electron image.

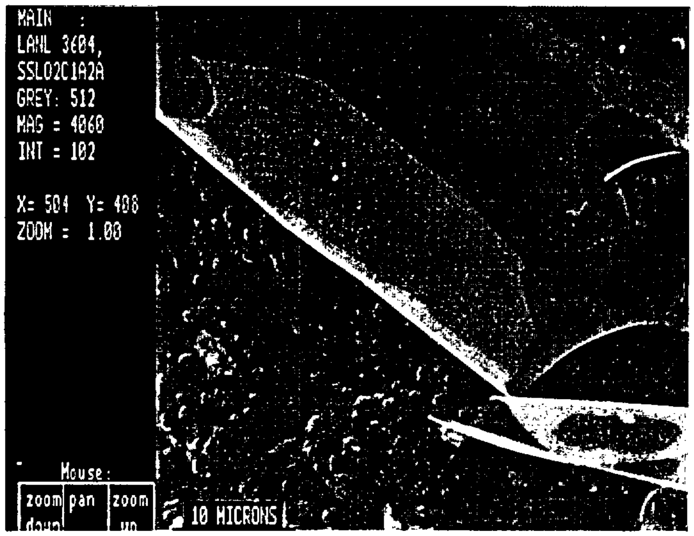

Figure 160 (file 17) Curled sheets of amorphous silica atop a small depression coated with earlier silica. Secondary-electron image.

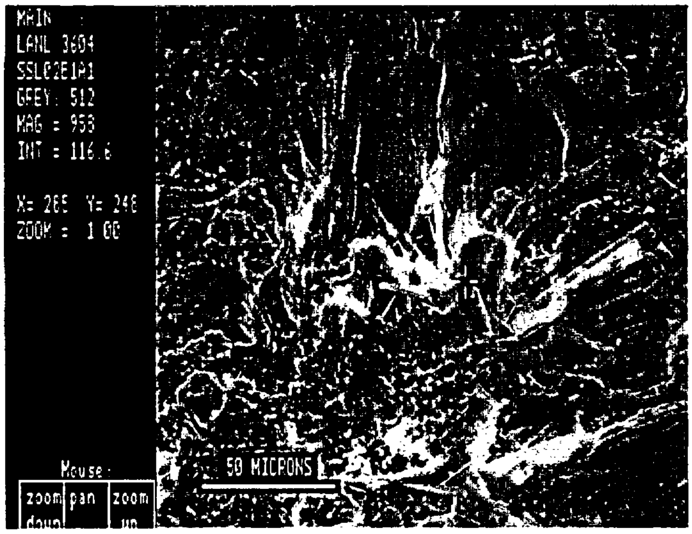

Figure 161 (file 16) Prismatic calcium sulfate. Secondary-electron image.

Figure 162 (file 11) Rounded mounds of probable calcite atop an earlier silica deposit. Secondary-electron image.

Figure 163 (file 4) Prismatic stellerite and other pre-test minerals engulfed by a lobate deposit of amorphous silica. Secondary-electron image.

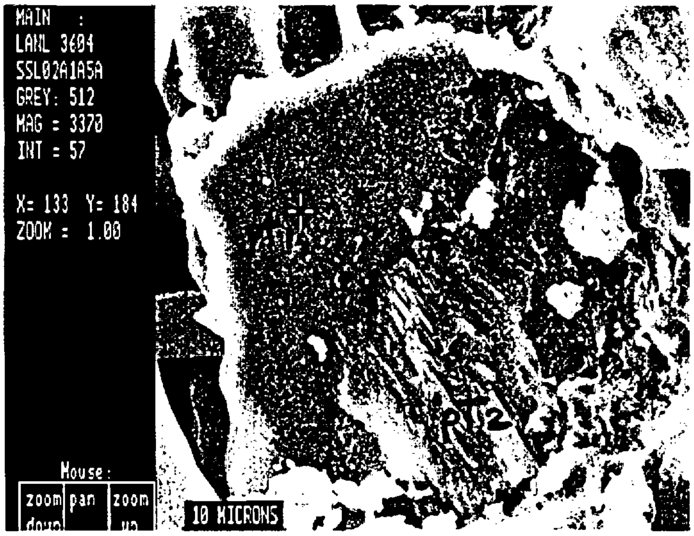

Figure 164 (file 10) Corroded pre-test crystals of stellerite (pt 2) and silica (pt 1) adjacent to the lobate deposit in Figure 163 (file 4). Secondary-electron image.

INTENTIONALLY LEFT BLANK

7. Drift Scale Test Heating/Cooling Schedule Revisited

Discussions were held during the June 8, 2001 workshop regarding the heater shut-off for the Drift Scale Test. Results from recent thermal calculations were presented that predicted heated drift wall temperatures of about 80 degrees C after 3 years of cooling. These predicted temperatures are shown in Figure 25.

Principal Investigators representing each of the three coupled process models presented their opinions. No one advocated extending the heating phase beyond the original 4 year plan. The Thermal-Chemical Process group requested 1 or 2 new core boreholes to investigate fluid reflux in the boiling zone shortly after shut-off. The Thermal-Mechanical group was interested in installing 5 tiltmeters in boreholes surrounding the heated drift. Tilitmeter boreholes would measure small movement in the rock following heater shut-off.

Drift Scale Test heater shut-off is a level 2 milestone as defined by the baseline plan. Unless preempted by new test information, workshop participants agreed that complete heater shut-off should proceed as originally planned with a slight delay to the beginning of 2002.

INTENTIONALLY LEFT BLANK

8. Planar Heat Source Design for the Cross Drift Thermal Test (CDTT)

The current design of the CDTT involves a planar heat source consisting of 11-rod heaters placed in parallel and spaced at 0.8 meters as shown generally in Figure 165. A 12th rod heater, parallel to the others, will be placed at 4.5 meters from one edge of the planar heat source. The current design should meet the same objectives as listed on page 6, Section 2.0 of the Cross Drift Thermal Test Planning Report published last August 2000. In addition to the broad objective of acquiring a better understanding of the coupled thermal-hydrological-mechanical-chemical processes in the near field of the lower lithophysal unit of Topopah Spring welded tuff, Section 2.0 of the planning report also listed a prioritized set of specific objectives. I shall address them one by one to show that not only have none of the stated objectives been compromised by the current design, but the THC aspect of the test objectives have been strengthened.

1. To test or investigate the premise that heat-mobilized pore water will shed/drain between emplacement drifts to below the repository horizon.

This objective will be met by the design of the 12th rod heater, and the horizontal drainage monitoring (temperature and neutron logging) boreholes placed at mid-point of 11th and 12th heater. The 12th heater is far enough away from the edge of the planar heat source so that the monitoring borehole will indeed be monitoring the drainage "between drifts". Another horizontal drainage monitoring borehole will be placed at within one meter of the 11th heater; this borehole will measure the drainage/shedding from the "repository edge". The heating power in 12th will be adjusted (based on TH modeling) to give rise to temperature gradient that is symmetrical about the mid-point of 11th and 12th heaters.

2. To test or investigate the premise that liquid water can penetrate through zones/regions at or above boiling temperature.

This objective is met by the design of the two temperature/neutron boreholes that have closely spaced temperature sensors between the elevation of the heater plane to 2.5 meters above the heater plane. Downward spikes of temperature from above boiling will be indicative of water penetrating through. The current design relies on temperature signatures for occurrence of water getting through. Temperature is the most sensitive measure, more so than geophysical measurements (which are volume averaged measures), and far more reliable that actual collection of water. This latter is because collection boreholes act as capillary barrier, therefore water collection in a borehole is only possible if there are local areas of full liquid saturation around the borehole. This is not very likely since drainage may increase the liquid saturation in the fractures only slightly. If water is not collected in the borehole it does not mean that drainage will not occur.

2 To measure the rock mass properties of the Tptpll.

This objective is not affected by the change of heat source design.

3 Chemistry of seepage water.

One of the motivation for changing the heat source to the current planar design is to ensure that there will be "prolonged" period of stable two-phase zone to insure that there can be repeated sampling of water. The placement of the three water collection boreholes at heights of 1.25 m, 2.0 m and 2.5 meters above the heater plane are at optimum elevations within these two-phase zones through the duration of heating.

4 Chemistry of gas.

This objective is not affected by the change of heat source design. The current plan also calls for sampling gas from the heater boreholes.

In summary, the current CDTT retains the objectives put forth in the planning document published August 2000. The modified design makes the test more efficient in construction, installation and implementation, and we are more likely to succeed in obtaining crucial data prior to LA.

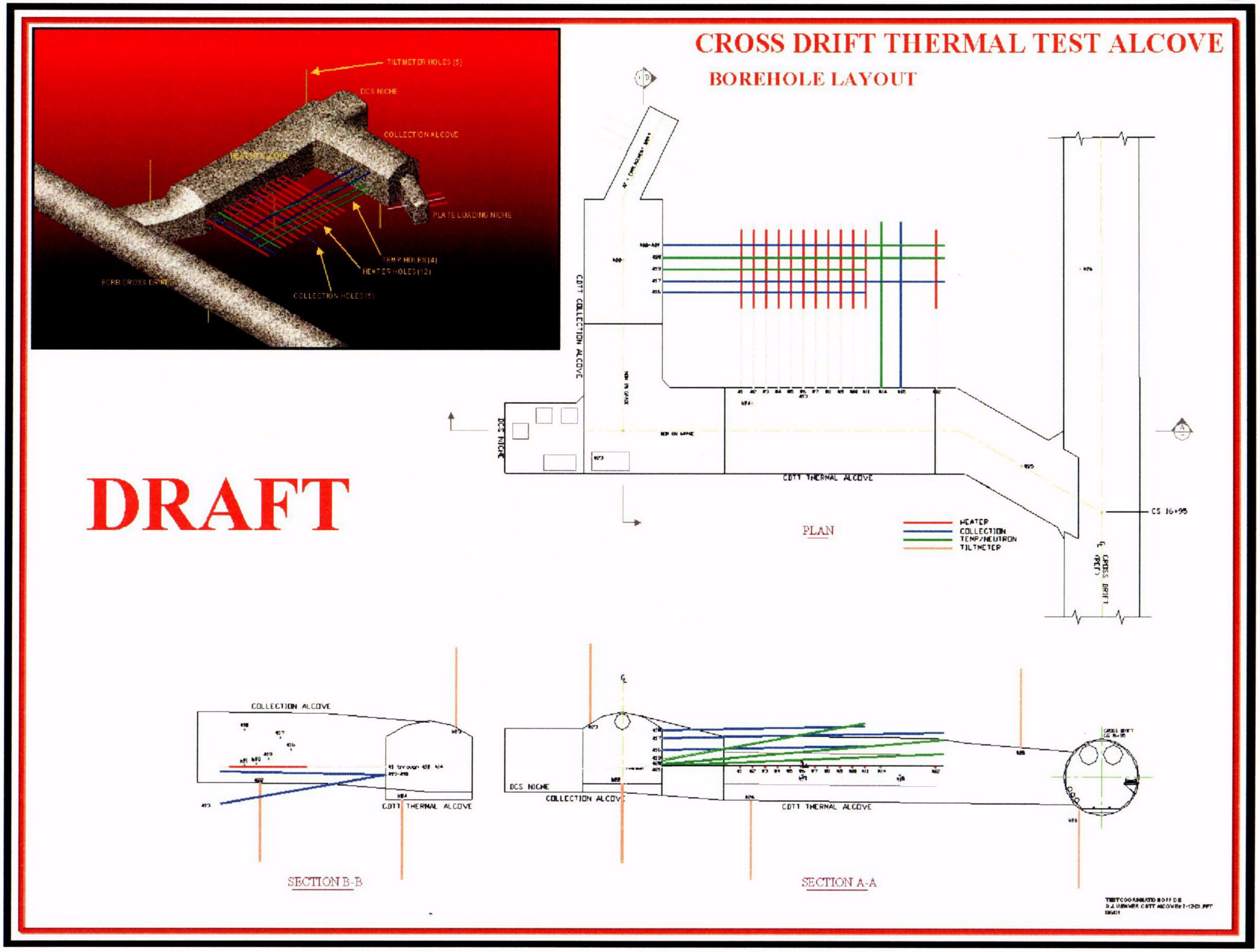

Figure 165. Preliminary Cross Drift Thermal Test Alcove Borehole Layout

INTENTIONALLY LEFT BLANK

9. DECOVALEX

9.1 GENERAL

DECOVALEX is an international consortium of governmental agencies associated with the management/disposal of high level nuclear waste and spent nuclear fuel in Canada, Germany, Japan, Finland, France, Spain, Sweden, the United Kingdom, and the United States. DECOVALEX stands for **DE**velopment of **CO**upled models and their **VAL**idation against **EX**periments, coinciding with the overall objective of the consortium. Simply stated the objective of DECOVALEX is validation of models which can be used to simulate thermal-hydrological-mechanical processes in the rock surrounding a nuclear waste repository.

DECOVALEX I, the first DECOVALEX project was from 1992 to 1995. The U.S. Nuclear Regulatory Commission was a participant in DECOVALEX I. DECOVALEX II was from 1995 to 1999. Both the Department of Energy's Yucca Mountain Site Characterization Office and the U.S. Nuclear Regulatory Commission joined DECOVALEX III which was started in 1999 and is expected to continue till 2002. In DECOVALEX III the Drift Scale Test at Yucca Mountain, which is a large scale, long term in-situ heater test, is a test case.

There are four tasks in DECOVALEX III. Task 1 is on the FEBEX test which is an engineered barrier system in-situ thermal test being conducted at the Grimsell site in Switzerland. The FEBEX test, sponsored by several European governmental agencies, is operated by ENRESA of Spain. Task 2 is on the YMP Drift Scale Test. Task 3 is on several topics such as coupled THM processes due to glaciation and homogenization or upscaling etc. Task 4 is a forum for DECOVALEX participants to interact with invited PA experts on the application of THM models in performance assessment.

The YMSCO is a participant in Task 1 and leads Task 2. It is also a participant in the BMT2 sub-task of Task 3. BSC provides technical support services on DECOVALEX including coordination of all activities and leading Task 2 studies. Currently, Task 1 modeling and analyses are assigned to Sandia National Laboratories, while Task 3 (BMT2) modeling and analyses are assigned to Lawrence Berkeley National Laboratory.

9.2 ACTIVITIES SINCE TOKAI WORKSHOP

Since the third DECOVALEX workshop was held in Tokai in January 2001 there was a Task 1 taskforce meeting in Madrid, Spain on May 22, 2001. Steve Sobolik of SNL attended this taskforce meeting. SNL have been doing simulations of laboratory-scale oedometer tests with Bentonite. SNL has also been developing a coupled version of the TOUGH2 and JAS3D codes.

On Task 2, BSC recently prepared the first draft of the Task 2A Interim Report and circulated it to Task 2A research teams for review. Task 2A Interim Report is expected to be completed by the time of the next workshop in Naantali, Finland in October 2001.

LBNL is currently performing phase II calculations on BMT2 and will present and discuss the results in the next workshop.

APPENDIX A

Drift Scale Test Index Figures and Information

This appendix contains index figures of test layouts, borehole configurations, and other general information familiar to the researchers but perhaps not familiar to all readers. It is important for the reader to understand that individual contributions contained herein may report locations in slightly different ways.

Boreholes may be referred to by one of two unique names: their numerical sequence number or by their functional sequence number. Table 1 of this appendix includes a list of boreholes numbers and names along with collar and bottom coordinates.

A local coordinate system has been established for each of the thermal tests to date. The DST coordinate system is shown in Figure 1 of this appendix. The 0,0,0 point is at the center of the heated drift bulkhead. The (0,0,0) coordinate for the DST is at: North 234,059.947, East 171,431.994, Elev. 1052.855 in Nevada State Plane Coordinates. The positive X axis extends approximately 18 degrees east of north and the positive Y axis extends 72 degrees west of north.

Another common data reporting method uses the distance along a borehole as measured from the collar of the borehole. Boreholes are generally oriented parallel to one of the axes of the coordinate system

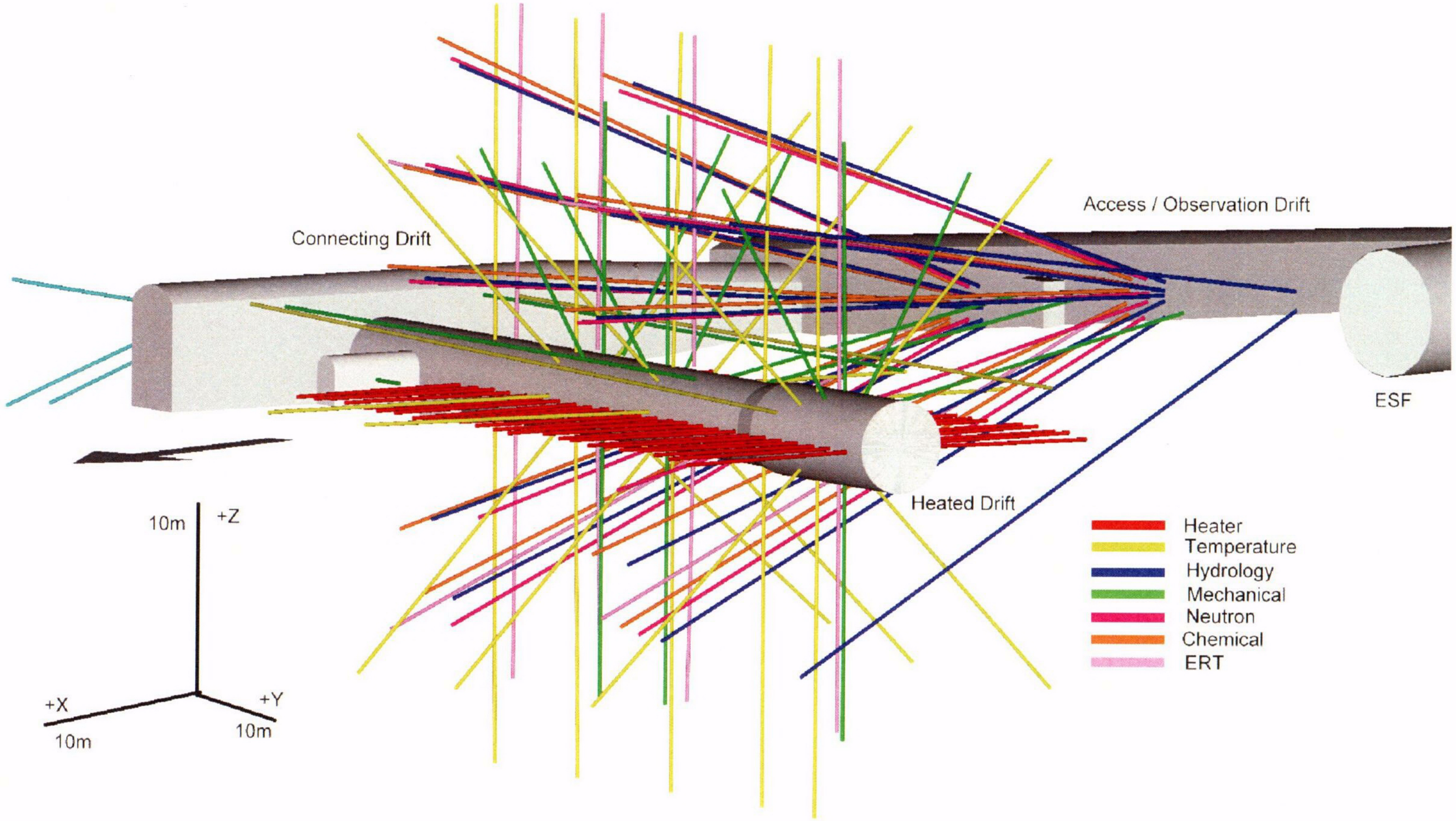

Figure 1. Perspective View Showing Drifts and Boreholes of the Drift Scale Test.

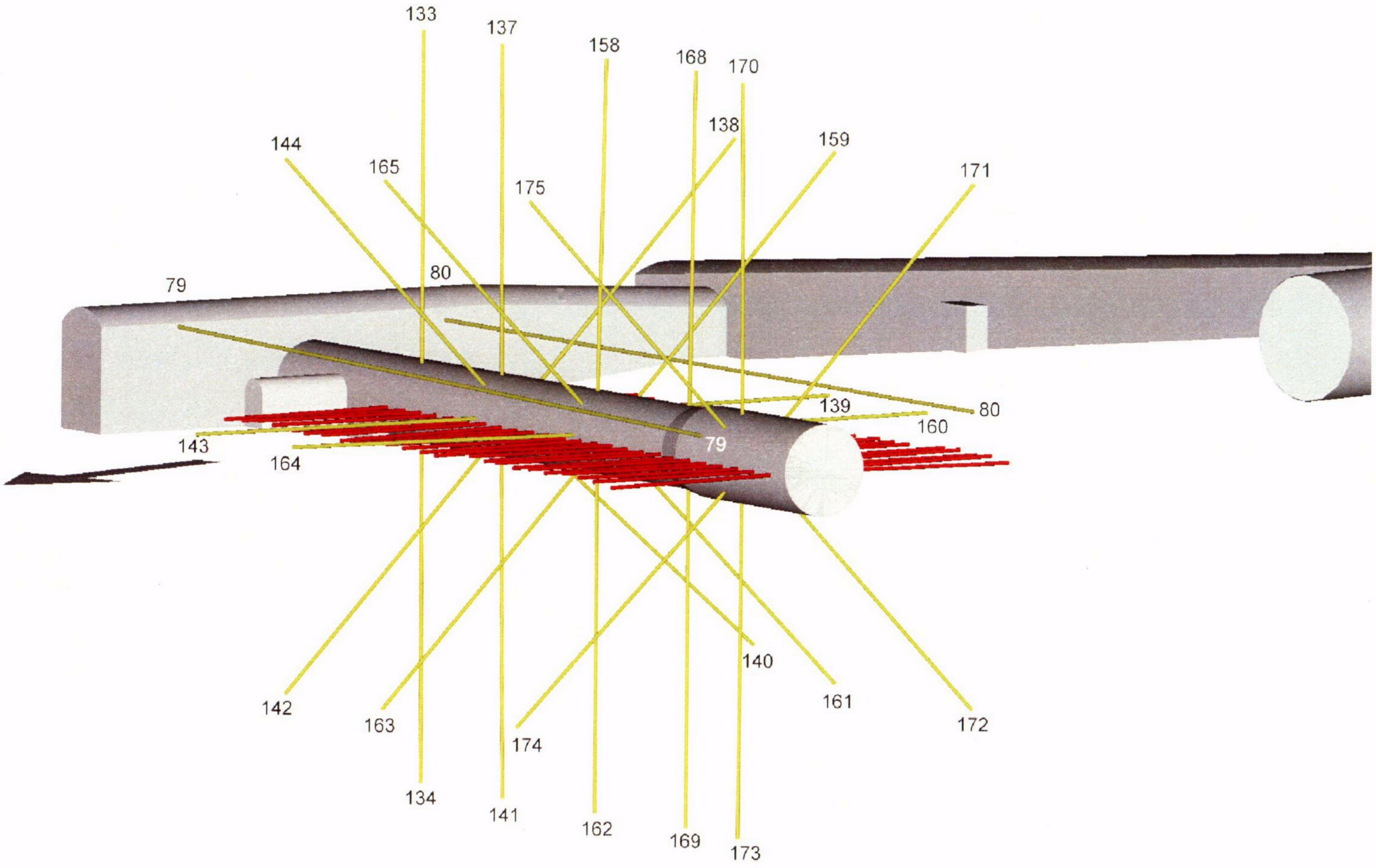

Figure 2. Perspective View Showing Temperature (RTD) Boreholes of the Drift Scale Test.

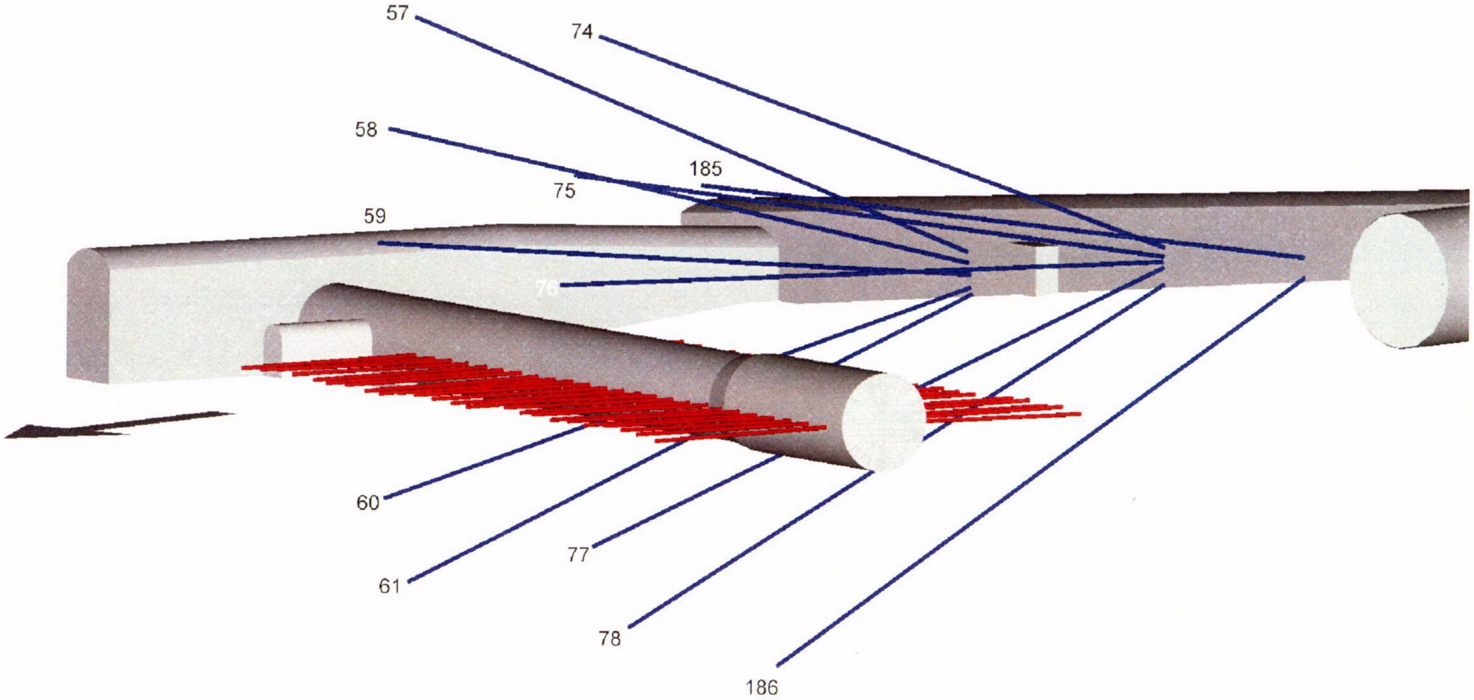

Figure 3. Perspective View Showing Hydrology Boreholes of the Drift Scale Test.

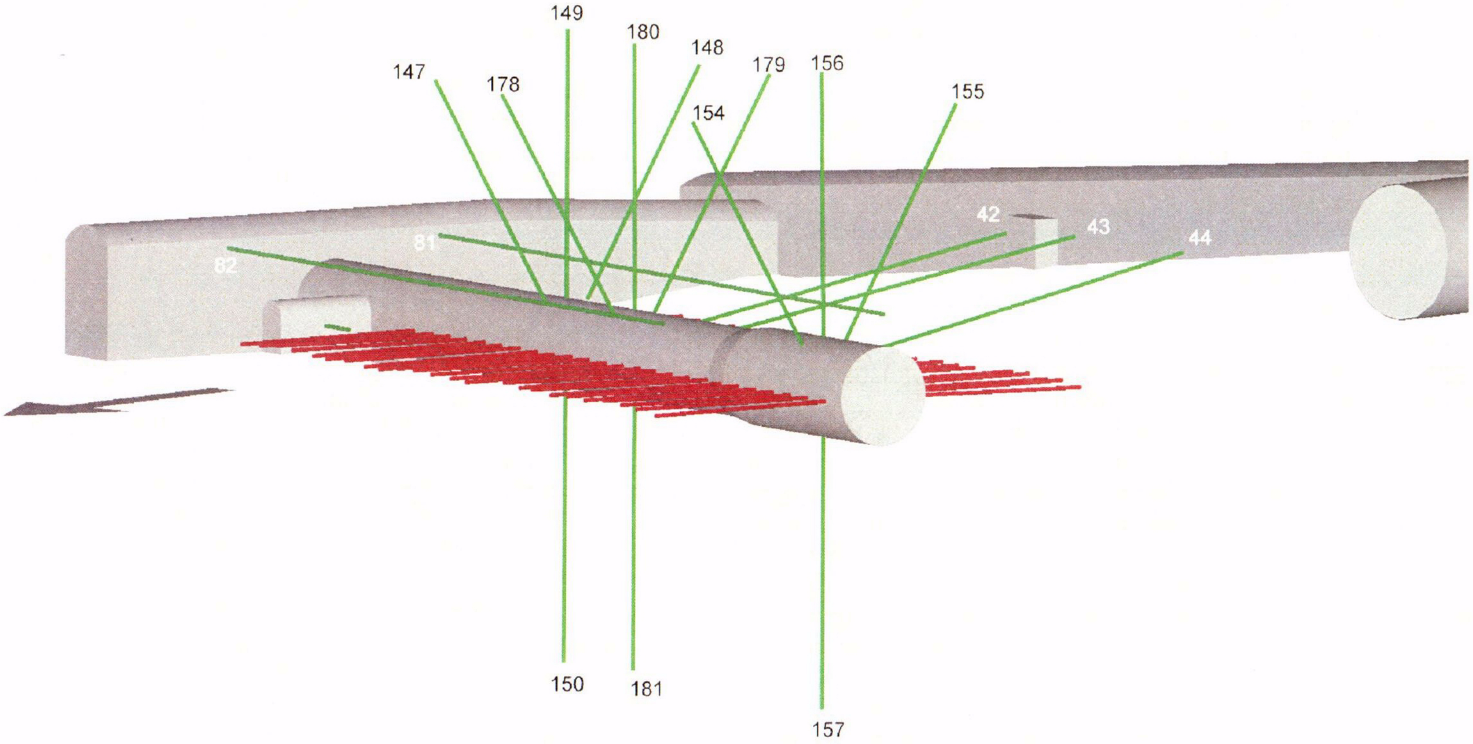

Figure 4. Perspective View Showing Mechanical (MPBX) Boreholes of the Drift Scale Test.

C-104

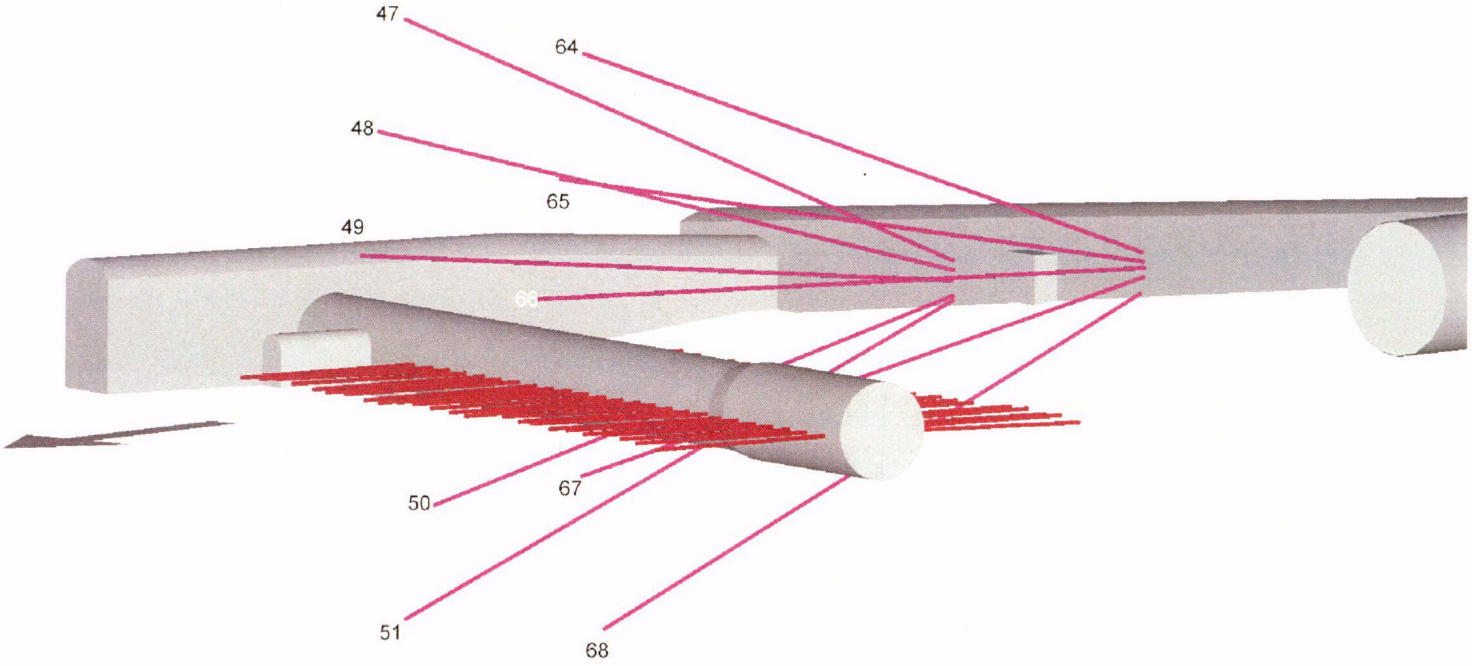

Figure 5. Perspective View Showing Neutron Boreholes of the Drift Scale Test.

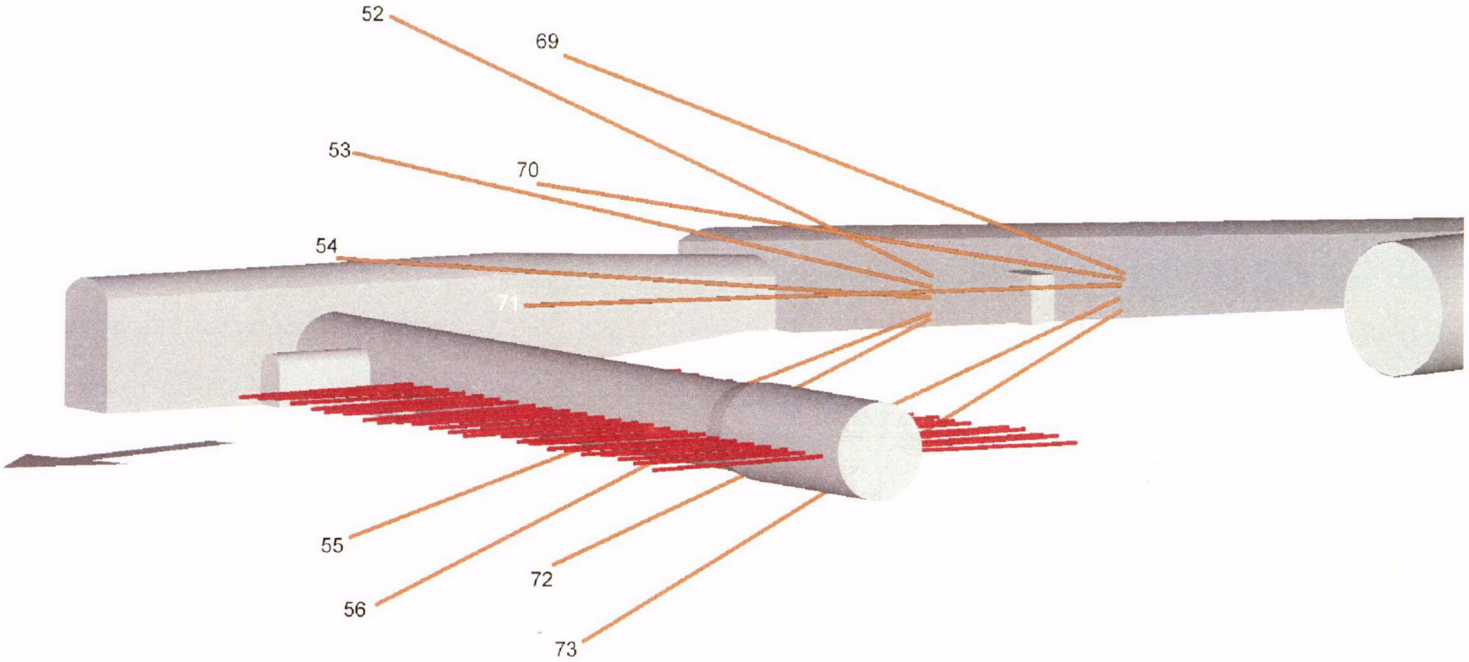

Figure 6. Perspective View Showing Chemical (SEAMIST) Boreholes of the Drift Scale Test.

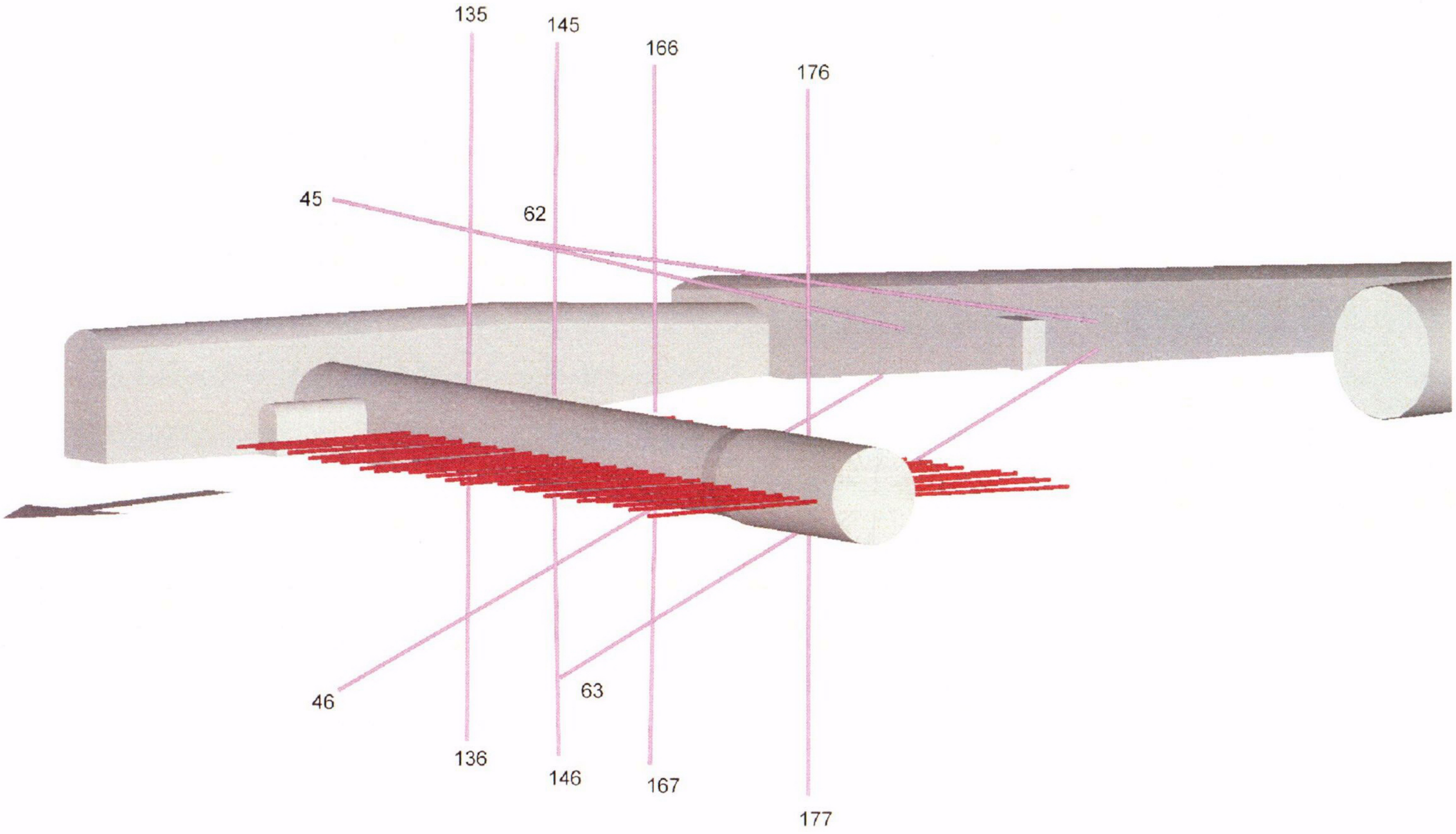

Figure 7. Perspective View Showing ERT Boreholes of the Drift Scale Test.

C-107

Table 1. Drift Scale Test Borehole Identification and Locations.

Borehole			Collar			Bottom			Diameter
Number	Identification	Primary Purpose	X (m)	Y (m)	Z (m)	X (m)	Y (m)	Z (m)	(cm)
42	ESF-SDM-42--MPBX-1	MPBX - Rock Mass Displacement	-29.3	13.8	4.6	-3.6	13.7	-0.4	7.7
43	ESF-SDM-43--MPBX-2	MPBX - Rock Mass Displacement	-29.2	21.1	5.1	-3.4	20.7	0.4	7.7
44	ESF-SDM-44--MPBX-3	MPBX - Rock Mass Displacement	-29.5	32.1	5.1	-3.6	32.2	-0.4	7.7
45	ESF-HD-45-ERT-1	Electrical Resistivity Tomography	-28.9	4.6	4.1	9.6	4.7	13.7	7.7
46	ESF-HD-46-ERT-2	Electrical Resistivity Tomography	-27.4	4.6	1.5	9.1	4.5	-14.3	7.7
47	ESF-HD-47-NEU-1	Neutron Probe	-29.1	6.4	4.6	7.2	6.3	21.1	7.7
48	ESF-HD-48-NEU-2	Neutron Probe	-29.1	6.4	4.0	9.5	6.3	13.5	7.7
49	ESF-HD-49-NEU-3	Neutron Probe	-29.0	6.4	3.4	10.8	6.7	7.7	7.7
50	ESF-HD-50-NEU-4	Neutron Probe	-29.0	6.4	2.6	9.7	6.4	-8.1	7.7
51	ESF-HD-51-NEU-5	Neutron Probe	-29.0	6.4	2.3	8.1	6.7	-12.0	7.7
52	ESF-HD-52-CHE-1	Chemistry - SEAMIST	-29.2	8.2	4.5	7.0	8.3	20.1	10.0
53	ESF-HD-53-CHE-2	Chemistry - SEAMIST	-29.2	8.3	4.0	9.4	8.7	13.9	10.0
54	ESF-HD-54-CHE-3	Chemistry - SEAMIST	-29.1	8.2	3.4	10.3	8.4	6.9	10.0
55	ESF-HD-55-CHE-4	Chemistry - SEAMIST	-29.2	8.2	2.6	5.1	8.0	-7.5	10.0
56	ESF-HD-56-CHE-5	Chemistry - SEAMIST	-29.2	8.2	2.3	7.3	8.5	-13.8	10.0
57	ESF-HD-57-HYD-1	Hydrology	-28.8	10.1	4.7	7.8	9.8	19.8	7.7
58	ESF-HD-58-HYD-2	Hydrology	-29.0	10.0	4.1	9.6	10.0	13.7	7.7
59	ESF-HD-59-HYD-3	Hydrology	-29.1	10.0	3.5	10.2	10.0	7.2	7.7
60	ESF-HD-60-HYD-4	Hydrology	-29.1	10.0	2.7	9.2	9.3	-7.3	7.7
61	ESF-HD-61-HYD-5	Hydrology	-29.2	10.1	2.3	8.2	10.2	-12.0	7.7
62	ESF-HD-62-ERT-3	Electrical Resistivity Tomography	-29.2	24.7	6.3	10.1	24.9	13.2	7.7
63	ESF-HD-63-ERT-4	Electrical Resistivity Tomography	-29.3	24.7	4.7	7.0	25.0	-11.9	7.7
64	ESF-HD-64-NEU-6	Neutron Probe	-29.3	26.5	6.6	8.1	26.4	20.8	7.7
65	ESF-HD-65-NEU-7	Neutron Probe	-29.3	26.5	6.3	9.9	26.7	13.7	7.7
66	ESF-HD-66-NEU-8	Neutron Probe	-29.1	26.5	6.0	10.7	26.6	6.9	7.7
67	ESF-HD-67-NEU-9	Neutron Probe	-29.0	26.5	5.2	8.3	25.9	-8.0	7.7
68	ESF-HD-68-NEU-10	Neutron Probe	-29.1	26.6	4.6	6.8	26.9	-12.3	7.7
69	ESF-HD-69-CHE-6	Chemistry - SEAMIST	-29.2	28.4	6.8	8.3	28.7	20.0	7.7

70	ESF-HD-70-CHE-7	Chemistry - SEAMIST	-29.3	28.4	6.3	10.0	29.0	13.1	7.7
71	ESF-HD-71-CHE-8	Chemistry - SEAMIST	-29.4	28.3	6.0	10.7	27.9	6.2	10.0
72	ESF-HD-72-CHE-9	Chemistry - SEAMIST	-29.3	28.4	5.5	8.4	28.8	-8.4	10.0
73	ESF-HD-73-CHE-10	Chemistry - SEAMIST	-29.1	28.4	4.5	6.6	28.5	-12.6	7.7
74	ESF-HD-74-HYD-6	Hydrology	-29.4	30.2	6.8	8.2	30.1	20.6	7.7
75	ESF-HD-75-HYD-7	Hydrology	-29.3	30.2	6.3	10.0	30.5	12.9	7.7
76	ESF-HD-76-HYD-8	Hydrology	-29.3	30.2	6.0	10.7	30.2	6.7	7.7
77	ESF-HD-77-HYD-9	Hydrology	-29.3	30.2	5.7	8.3	29.9	-8.2	7.7
78	ESF-HD-78-HYD-10	Hydrology	-29.4	30.2	4.7	6.5	30.4	-12.9	7.7
79	ESF-HD-79-TEMP-1	Temperature	9.5	-11.0	3.8	9.5	48.5	2.7	10.0
80	ESF-HD-80-TEMP-2	Temperature	-9.5	-11.1	3.2	-9.9	48.6	3.2	10.0
81	ESF-HD-81-MPBX-1	MPBX - Rock Mass Displacement	7.0	-11.1	3.5	6.8	34.9	3.3	7.7
82	ESF-HD-82-MPBX-2	MPBX - Rock Mass Displacement	-7.0	-11.0	3.5	-7.7	35.3	3.1	7.7
83	ESF-HD-83-WH-1	Wing Heater	-2.5	1.8	-0.3	-14.0	1.8	-0.3	10.0
84	ESF-HD-84-WH-2	Wing Heater	-2.5	3.6	-0.2	-14.0	3.7	-0.2	10.0
85	ESF-HD-85-WH-3	Wing Heater	-2.5	5.5	-0.2	-14.1	5.5	-0.3	10.0
86	ESF-HD-86-WH-4	Wing Heater	-2.5	7.3	-0.3	-13.9	7.2	-0.4	10.0
87	ESF-HD-87-WH-5	Wing Heater	-2.6	9.2	-0.3	-14.0	9.3	-0.2	10.0
88	ESF-HD-88-WH-6	Wing Heater	-2.6	11.0	-0.2	-14.0	10.9	-0.2	10.0
89	ESF-HD-89-WH-7	Wing Heater	-2.8	12.8	-0.2	-14.0	12.9	-0.3	10.0
90	ESF-HD-90-WH-8	Wing Heater	-2.5	14.6	-0.3	-14.1	14.5	-0.4	10.0
91	ESF-HD-91-WH-9	Wing Heater	-2.5	16.5	-0.2	-13.8	16.6	-0.2	10.0
92	ESF-HD-92-WH-10	Wing Heater	-2.5	18.3	-0.3	-14.1	18.2	-0.3	10.0
93	ESF-HD-93-WH-11	Wing Heater	-2.4	20.1	-0.3	-14.0	20.1	-0.5	10.0
94	ESF-HD-94-WH-12	Wing Heater	-2.5	22.0	-0.2	-13.9	22.1	-0.2	10.0
95	ESF-HD-95-WH-13	Wing Heater	-2.6	23.8	-0.3	-14.1	23.8	-0.3	10.0
96	ESF-HD-96-WH-14	Wing Heater	-2.6	25.6	-0.3	-14.1	25.7	-0.6	10.0
97	ESF-HD-97-WH-15	Wing Heater	-2.5	27.5	-0.2	-14.1	27.6	-0.4	10.0
98	ESF-HD-98-WH-16	Wing Heater	-2.4	29.2	-0.2	-13.6	29.2	-0.3	10.0
99	ESF-HD-99-WH-17	Wing Heater	-2.6	31.1	-0.3	-14.0	31.3	-0.3	10.0
100	ESF-HD-100-WH-18	Wing Heater	-2.5	32.9	-0.2	-14.0	33.0	-0.3	10.0
101	ESF-HD-101-WH-19	Wing Heater	-2.7	34.7	-0.3	-14.1	34.7	-0.3	10.0

102	ESF-HD-102-WH-20	Wing Heater	-2.6	36.6	-0.3	-14.0	36.4	-0.6	10.0
103	ESF-HD-103-WH-21	Wing Heater	-2.6	38.4	-0.2	-14.2	38.5	-0.2	10.0
104	ESF-HD-104-WH-22	Wing Heater	-2.6	40.2	-0.3	-14.1	40.3	-0.1	10.0
105	ESF-HD-105-WH-23	Wing Heater	-2.6	42.1	-0.3	-14.1	42.2	-0.2	10.0
106	ESF-HD-106-WH-24	Wing Heater	-2.6	43.9	-0.2	-14.1	43.9	-0.2	10.0
107	ESF-HD-107-WH-25	Wing Heater	-2.6	45.7	-0.3	-14.2	45.8	-0.4	10.0
108	ESF-HD-108-WH-26	Wing Heater	2.6	45.7	-0.3	14.1	45.8	-0.5	10.0
109	ESF-HD-109-WH-27	Wing Heater	2.6	43.9	-0.3	14.1	43.8	-0.3	10.0
110	ESF-HD-110-WH-28	Wing Heater	2.6	42.1	-0.3	14.1	42.1	-0.2	10.0
111	ESF-HD-111-WH-29	Wing Heater	2.6	40.2	-0.2	14.1	40.3	-0.1	10.0
112	ESF-HD-112-WH-30	Wing Heater	2.6	38.4	-0.3	14.2	38.3	-0.3	10.0
113	ESF-HD-113-WH-31	Wing Heater	2.6	36.6	-0.2	14.1	36.5	-0.2	10.0
114	ESF-HD-114-WH-32	Wing Heater	2.9	34.8	-0.3	14.3	35.0	-0.3	10.0
115	ESF-HD-115-WH-33	Wing Heater	2.6	32.9	-0.2	14.1	32.7	-0.2	10.0
116	ESF-HD-116-WH-34	Wing Heater	2.7	31.1	-0.3	13.9	31.0	-0.2	10.0
117	ESF-HD-117-WH-35	Wing Heater	2.6	29.2	-0.2	13.8	29.2	-0.1	10.0
118	ESF-HD-118-WH-36	Wing Heater	2.6	27.4	-0.2	14.2	27.4	0.0	10.0
119	ESF-HD-119-WH-37	Wing Heater	2.5	25.6	-0.3	14.1	25.7	-0.4	10.0
120	ESF-HD-120-WH-38	Wing Heater	2.5	23.8	-0.3	14.0	23.8	-0.4	10.0
121	ESF-HD-121-WH-39	Wing Heater	2.5	21.9	-0.3	14.1	21.9	-0.3	10.0
122	ESF-HD-122-WH-40	Wing Heater	2.5	20.1	-0.2	14.1	20.1	-0.2	10.0
123	ESF-HD-123-WH-41	Wing Heater	2.5	18.3	-0.2	14.1	18.3	-0.3	10.0
124	ESF-HD-124-WH-42	Wing Heater	2.5	16.4	-0.3	14.0	16.3	-0.5	10.0
125	ESF-HD-125-WH-43	Wing Heater	2.5	14.6	-0.3	14.0	14.7	-0.5	10.0
126	ESF-HD-126-WH-44	Wing Heater	2.5	12.8	-0.2	14.1	12.9	-0.3	10.0
127	ESF-HD-127-WH-45	Wing Heater	2.6	10.9	-0.3	14.1	10.7	-0.4	10.0
128	ESF-HD-128-WH-46	Wing Heater	2.5	9.1	-0.3	14.0	9.2	-0.4	10.0
129	ESF-HD-129-WH-47	Wing Heater	2.6	7.3	-0.2	14.1	7.1	-0.3	10.0
130	ESF-HD-130-WH-48	Wing Heater	2.6	5.5	-0.2	14.0	5.4	-0.2	10.0
131	ESF-HD-131-WH-49	Wing Heater	2.6	3.7	-0.3	14.1	3.7	-0.3	10.0
132	ESF-HD-132-WH-50	Wing Heater	2.6	1.8	-0.3	14.0	1.6	-0.4	10.0
133	ESF-HD-133-TEMP-3	Temperature	0.7	2.7	2.4	0.9	2.8	22.5	7.7

134	ESF-HD-134-TEMP-4	Temperature	0.7	2.7	-1.6	0.6	2.8	-22.9	7.7
135	ESF-HD-135-ERT-5	Electrical Resistivity Tomography	-0.8	2.7	2.4	-1.0	2.8	22.4	7.7
136	ESF-HD-136-ERT-6	Electrical Resistivity Tomography	-0.8	2.7	-1.6	-0.7	2.6	-18.0	7.7
137	ESF-HD-137-TEMP-5	Temperature	0.8	11.9	2.5	0.9	11.8	22.5	7.7
138	ESF-HD-138-TEMP-6	Temperature	-2.0	11.9	2.0	-16.0	11.5	15.9	7.7
139	ESF-HD-139-TEMP-7	Temperature	-2.6	11.9	0.0	-22.5	12.0	0.1	7.7
140	ESF-HD-140-TEMP-8	Temperature	-1.9	11.9	-1.6	-17.4	11.8	-14.7	7.7
141	ESF-HD-141-TEMP-9	Temperature	0.8	11.9	-1.6	0.6	12.0	-23.0	7.7
142	ESF-HD-142-TEMP-10	Temperature	1.6	11.9	-1.6	16.0	11.9	-15.9	7.7
143	ESF-HD-143-TEMP-11	Temperature	2.7	11.9	0.0	22.5	11.9	0.0	7.7
144	ESF-HD-144-TEMP-12	Temperature	2.0	11.9	2.0	16.4	12.1	16.4	7.7
145	ESF-HD-145-ERT-7	Electrical Resistivity Tomography	-0.8	11.9	2.6	-0.9	12.0	22.7	7.7
146	ESF-HD-146-ERT-8	Electrical Resistivity Tomography	-0.8	11.9	-1.6	-1.1	11.9	-18.0	7.7
147	ESF-HD-147-MPBX-3	MPBX - Rock Mass Displacement	1.3	13.7	2.2	8.7	13.7	15.2	7.7
148	ESF-HD-148-MPBX-4	MPBX - Rock Mass Displacement	-1.4	13.7	2.4	-8.9	13.7	15.2	7.7
149	ESF-HD-149-MPBX-5	MPBX - Rock Mass Displacement	0.0	13.7	2.5	-0.1	13.6	17.6	7.7
150	ESF-HD-150-MPBX-6	MPBX - Rock Mass Displacement	0.0	13.7	-1.6	0.1	13.8	-18.0	7.7
151	ESF-HD-151-REKA-1	Thermal Conductivity and Diffusivity	0.0	17.4	2.7	0.0	17.3	12.7	4.8
152	ESF-HD-152-REKA-2	Thermal Conductivity and Diffusivity	-2.4	17.4	0.0	-12.5	17.2	0.1	4.8
153	ESF-HD-153-REKA-3	Thermal Conductivity and Diffusivity	-1.6	17.4	-1.6	-9.2	17.2	-9.3	4.8
154	ESF-HD-154-MPBX-7	MPBX - Rock Mass Displacement	1.3	21.0	2.2	8.9	21.0	15.1	7.7
155	ESF-HD-155-MPBX-8	MPBX - Rock Mass Displacement	-1.3	21.0	2.3	-9.0	20.9	15.3	7.7
156	ESF-HD-156-MPBX-9	MPBX - Rock Mass Displacement	0.0	21.0	2.5	0.0	20.9	17.5	7.7
157	ESF-HD-157-MPBX-10	MPBX - Rock Mass Displacement	0.0	21.0	-1.6	0.0	21.0	-17.8	7.7
158	ESF-HD-158-TEMP-13	Temperature	0.8	22.8	2.6	0.4	23.0	22.6	7.7
159	ESF-HD-159-TEMP-14	Temperature	-1.9	22.9	1.9	-16.0	22.9	16.2	7.7
160	ESF-HD-160-TEMP-15	Temperature	-2.5	22.9	0.0	-22.6	23.0	0.1	7.7
161	ESF-HD-161-TEMP-16	Temperature	-1.6	22.9	-1.6	-16.0	23.2	-15.9	7.7
162	ESF-HD-162-TEMP-17	Temperature	0.8	22.9	-1.6	0.8	23.0	-22.8	7.7
163	ESF-HD-163-TEMP-18	Temperature	1.5	22.8	-1.6	15.8	22.5	-15.9	7.7
164	ESF-HD-164-TEMP-19	Temperature	2.5	22.9	0.0	22.6	23.0	0.3	7.7
165	ESF-HD-165-TEMP-20	Temperature	1.9	22.8	1.9	16.0	22.8	16.0	7.7

166	ESF-HD-166-ERT-9	Electrical Resistivity Tomography	-0.7	22.8	2.6	-0.6	23.0	22.4	7.7
167	ESF-HD-167-ERT-10	Electrical Resistivity Tomography	-0.8	22.8	-1.6	-0.5	22.7	-17.5	7.7
168	ESF-HD-168-TEMP-21	Temperature	-0.1	32.0	2.5	-0.3	32.0	22.7	7.7
169	ESF-HD-169-TEMP-22	Temperature	0.0	32.0	-1.6	0.3	32.4	-22.9	7.7
170	ESF-HD-170-TEMP-23	Temperature	0.8	39.3	2.5	0.7	39.1	22.6	7.7
171	ESF-HD-171-TEMP-24	Temperature	-1.9	39.3	1.8	-15.6	39.3	15.7	7.7
172	ESF-HD-172-TEMP-25	Temperature	-1.6	39.3	-1.6	-16.0	38.9	-16.0	7.7
173	ESF-HD-173-TEMP-26	Temperature	0.8	39.3	-1.6	0.7	39.1	-22.9	7.7
174	ESF-HD-174-TEMP-27	Temperature	1.6	39.3	-1.6	16.4	38.9	-15.4	7.7
175	ESF-HD-175-TEMP-28	Temperature	1.9	39.3	1.8	15.9	39.2	16.3	7.7
176	ESF-HD-176-ERT-11	Electrical Resistivity Tomography	-0.8	39.3	2.5	-0.8	39.1	22.5	7.7
177	ESF-HD-177-ERT-12	Electrical Resistivity Tomography	-0.7	39.3	-1.6	-0.7	39.3	-17.8	7.7
178	ESF-HD-178-MPBX-11	MPBX - Rock Mass Displacement	1.3	41.1	2.2	8.7	41.1	15.3	7.7
179	ESF-HD-179-MPBX-12	MPBX - Rock Mass Displacement	-1.3	41.1	2.3	-8.8	41.1	15.4	7.7
180	ESF-HD-180-MPBX-13	MPBX - Rock Mass Displacement	0.0	41.1	2.6	0.1	41.1	17.7	7.7
181	ESF-HD-181-MPBX-14	MPBX - Rock Mass Displacement	0.0	41.2	-1.7	0.1	41.2	-18.1	7.7
182	ESF-HD-182-PERM-1	Ambient Characterization	11.6	-15.7	2.3	12.0	-34.5	-4.4	7.7
183	ESF-HD-183-PERM-2	Ambient Characterization	10.7	-15.6	3.0	10.9	-35.7	3.0	7.7
184	ESF-HD-184-PERM-3	Ambient Characterization	8.9	-15.7	2.3	8.9	-34.5	-4.4	7.7
185	ESF-HD-185-HYD-11	Hydrology	-29.5	44.7	7.6	10.1	44.1	13.6	7.7
186	ESF-HD-186-HYD-12	Hydrology	-29.6	44.8	6.5	5.0	44.4	-13.8	7.7
187	ESF-PL-187-MPBX-1	MPBX - Rock Mass Displacement	5.5	-5.1	-0.3	5.5	-8.5	-0.4	7.7
188	ESF-PL-188-MPBX-2	MPBX - Rock Mass Displacement	5.5	-2.8	-0.3	5.5	0.5	-0.3	7.7